PCCP

PAPER

View Article Online
View Journal | View Issue

Cite this: *Phys. Chem. Chem. Phys.*, 2014, **16**, 25989

The influence of intercalated oxygen on the properties of graphene on polycrystalline Cu under various environmental conditions†

Raoul Blume,*[a] Piran R. Kidambi,[bc] Bernhard C. Bayer,[bd] Robert S. Weatherup,[b] Zhu-Jun Wang,[e] Gisela Weinberg,[e] Marc-Georg Willinger,[e] Mark Greiner,[e] Stephan Hofmann,[b] Axel Knop-Gericke[e] and Robert Schlögl[e]

Received 8th September 2014,
Accepted 23rd October 2014

DOI: 10.1039/c4cp04025b

www.rsc.org/pccp

Intercalation of oxygen at the interface of graphene grown by chemical vapour deposition and its polycrystalline copper catalyst can have a strong impact on the electronic, chemical and structural properties of both the graphene and the Cu. This can affect the oxidation resistance of the metal as well as subsequent graphene transfer. Here, we show, using near ambient pressure X-ray photoelectron spectroscopy (NAP-XPS), X-ray absorption near edge spectroscopy (XANES), energy dispersive X-ray spectroscopy (EDX) and (environmental) scanning electron microscopy (ESEM) that both the oxygen intercalation and de-intercalation are kinetically driven and can be clearly distinguished from carbon etching. The obtained results reveal that a charge transfer between as grown graphene and Cu can be annulled by intercalating oxygen creating quasi-free-standing graphene. This effect is found to be reversible on vacuum annealing proceeding *via* graphene grain boundaries and defects within the graphene but not without loss of graphene by oxidative etching for repeated (de-)intercalation cycles.

Introduction

Because of its unique electrical, mechanical, surface and thermal properties a single layer of sp^2 bonded carbon, also known as graphene or, in order to allow a more versatile discrimination between a monolayer and graphite, mono layer graphene (MLG), is considered as an interesting material for next generation electronics, optoelectronics and microsystems. In this context, catalytic chemical vapour deposition (CVD) has emerged as the most promising synthesis technique to achieve the required large scale graphene growth and control over its properties. In CVD, the development, characterization and optimization of suitable catalyst/carbon source combinations for MLG and few layer graphene (FLG) growth have recently received a lot of research interest.[1–8] Polycrystalline Cu exposed to gaseous hydrocarbons has emerged as the prime combination of catalyst and carbon source, as this yields good MLG growth results at scalable, industrially relevant conditions of temperature and gas pressure.[6] However, its quality still suffers from the presence of grain boundaries and all sorts of defects, both obstacles which have to be overcome to meet technical requirements.

Previous work on graphene CVD on polycrystalline Cu using near ambient pressure X-ray photoelectron spectroscopy (NAP-XPS) *in situ* during MLG growth revealed a distinct difference in the C1s binding energy (BE) values of *in situ* grown MLG and MLG that has been exposed to air.[9] This difference manifested itself as C1s binding energies at 284.75 eV (growth) and 284.4 eV (exposed to air), the latter of which matches the commonly reported value of graphitic carbon. We have previously attributed this BE shift between as grown and air exposed MLG on Cu to differences in charge transfer between substrate and graphene

[a] *Helmholtz-Zentrum Berlin für Materialien und Energie, Albert-Einstein-Str. 15, D-12489 Berlin, Germany. E-mail: raoul@fhi-berlin.mpg.de; Tel: +49(0)30806214024*
[b] *Department of Engineering, University of Cambridge, 9 JJ Thomson Avenue, Cambridge CB3 0FA, UK. E-mail: sh315@cam.ac.uk*
[c] *Mechanical Engineering Department, Massachusetts Institute of Technology, 77 Massachusetts Avenue, Cambridge MA 02139-4307, USA*
[d] *Faculty of Physics, University of Vienna, Boltzmanngasse 5, A-1090 Wien, Austria. E-mail: bernhard.bayer@univie.ac.at*
[e] *Fritz-Haber-Institut der Max-Planck-Gesellschaft, Faradayweg 4-6, D-14195 Berlin-Dahlem, Germany. E-mail: acsek@fhi-berlin.mpg.de*

† Electronic supplementary information (ESI) available: Table of T–R-cycling procedures on samples included in this paper; Raman spectra of fresh, three times and five times cycled GF/Cu surfaces; SEM micrographs and corresponding EDX spectra of a five times cycled GF/Cu surface; SEM micrographs and corresponding EDX spectra of SiO_2 grains on fresh GF/Cu; overview of depth resolved, fitted O1s spectra of three times cycled GF/Cu during cycling; details of the evolution of the fitted C1s region of GF/Cu during thermally activated intercalation of and etching by oxygen at different oxygen pressures; Arrhenius plots of de-intercalation of oxygen of GF/Cu by heating to 600 °C; evolution of the Cu LMM and O1s spectra of FLG during heating to 600 °C and subsequent cooling to RT; evolution of the WF of a five times cycled GF/Cu sample during cycle 4 and 5; ESEM movie corresponding to Fig. 3. See DOI: 10.1039/c4cp04025b

caused by the presence–absence of presumably intercalated oxygen atoms.[9] Similar effects in the presence of *e.g.* oxygen, H_2O or CO were recently reported for graphene on several transition metals.[10–26]

However, in the case of MLG on Cu it is still under investigation whether only intercalated oxygen is responsible for the observed BE differences and to what extent other effects such as oxidation of the catalyst or even those related to the experimental method are also involved. In the context of XPS where photoelectrons are created the intercalation of oxygen or oxidation of the catalyst would reflect a ground state phenomenon. On the other hand detected shifts may also be related to screening final state effects. The observed reduced binding energies after air exposure may prove an important issue when transferring as grown graphene on other substrates because it can facilitate the lift off process as has been shown for graphene on Pt.[27] In contrast, intercalating oxygen may affect the chemical stability of MLG and the metal it is contacting, an effect which could be amplified by applying even moderate heat as could happen in applications such as integrated devices. For such applications it is essential to have environmentally resistant metal contacts and graphene of defined electronic properties, especially when using Cu.[28–33] Also changes in charge transfer from the substrate may unintentionally dope the graphene, which is problematic for devices which require a certain band structure alignment.[34,35] Equally, MLG-support interactions may also impact on graphene's debated wetting transparency and potential use as a corrosion barrier.[36–43]

In our previous work, we focused mainly on mechanisms leading to MLG growth without extending the discussion of the oxygen induced charge transfer further.[9] Hence, the aim of the present investigation is to gain more detailed insight into the nature of oxygen intercalation and its influence on a charge transfer and BE shift, respectively. For this purpose, we compare the evolution of Cu-grown graphene flakes (GF) with continuous MLG films during oxidation–reduction cycles. GFs with low coverage are used to enhance the intercalation process and its reversibility by heating due to potentially shorter diffusion lengths involved, thereby engineering a model system to observe these effects more clearly. Activation energies of oxygen intercalation and oxidation of graphene were determined by heating GF on Cu in an oxygen atmosphere at different pressures. Repeated cycles of reduction in vacuum and re-oxidation in oxygen/air of GF and MLG on Cu were undertaken to gain insights into long term stability effects and sample aging. *In situ* characterization was performed with near ambient pressure X-ray photoelectron spectroscopy (NAP-XPS), X-ray absorption near edge spectroscopy (XANES), environmental scanning electron microscopy (ESEM). Due to its usefulness in estimating charge transfers whilst being notoriously difficult to measure *via* electrical characterization, we also determine the work function (WF) of graphene on Cu by photoelectron-based measurements.[13,17,30] Corresponding reference characterizations were performed *ex situ* by scanning electron microscopy (SEM), energy dispersive X-ray spectroscopy (EDX) and Raman spectroscopy.

Experimental

Graphene growth was performed by chemical vapour deposition (CVD) of benzene (C_6H_6, vapour pressure $\sim 1 \times 10^{-3}$ mbar, 99.2% purity) as a carbon precursor in a customized cold wall low pressure reactor. The catalyst material was 25 μm commercially available polycrystalline Cu foil (Alfa Aesar Puratronic, 99.999% purity). Details on growth condition and recipes can be found in ref. 6. Several samples covered with continuous MLG (domain sizes up to 20 μm), continuous FLG ($\approx$3–4 layers) or many isolated mono layer graphene flakes (GF; domain sizes 10 to 20 μm) samples were prepared. The samples were characterized with Raman spectroscopy (Renishaw InVia spectrometer, 532 nm excitation; ref. 6 and 9 and ESI,† Fig. S1).

Cycles of reduction and reoxidation were conducted by heating the samples *in situ* in vacuum (base pressure $\approx 10^{-8}$ mbar) and, *ex situ*, by subsequent exposure to ambient air at room temperature. The cycles are labelled T(emperature)–R(eoxidation)-cycling throughout the text. A detailed overview of the applied conditions is given in ESI,† Table S1. Activation experiments were performed *in situ* by stepwise heating the samples from room temperature (RT) up to 600 °C in oxygen atmosphere at $p_{O_2} = 5 \times 10^{-5}$, 5×10^{-2} and 0.2 mbar, respectively. Activation energies were directly derived from XP spectra following the procedure of Tjandra and Zaera.[44]

The near ambient pressure XPS experiments were performed at the ISISS beamline of the FHI located at the BESSY II synchrotron radiation facility in Berlin. The setup consists of a reaction cell attached to a set of differentially pumped electrostatic lenses and a separately pumped analyzer (Phoibos 150 Plus, SPECS GmbH), as described elsewhere.[45] The spectra were collected in normal emission in vacuum with a probe size of $\approx$150 μm $\times$ 80 μm. The samples were heated from the back using an external IR-laser (cw, 808 nm). The temperature was controlled *via* a K-type thermocouple in direct contact with the sample surface. Possible sample contamination was checked by survey spectra at the beginning of each experiment. In order to obtain depth resolved information, the photo electron spectra were taken at two different photon energies for each element, specifically 1400 eV/1080 eV (Cu2p, CuLMM), 980 eV/680 eV (O1s) and 725 eV/425 eV (C1s), with a spectral resolution of $\approx$0.3 eV. The respective kinetic energies of the electrons correspond to an electron mean free path of $\approx$12 Å and 7 Å. The total XPS information depths are $\approx$2 nm and $\approx$4 nm, that is, 95% of all detected electrons originate from 3λ.[46] For XPS analysis, the photoelectron binding energy (BE) is referenced to the Fermi edge, and the spectra are normalized to the incident photon flux. The photoionization cross section was considered according to the calculations of Yeh and Lindau.[47] Background correction was performed by using a Shirley background.[48] The spectra were fitted following the Levenberg–Marquardt algorithm to minimize the χ^2. Peak shapes were modelled by using Doniach–Sùnjić functions convoluted with Gaussian profiles so that an asymmetric line shape could be fitted when required.[49] The accuracy of the fitted peak positions is $\approx$0.05 eV. An overview of the fitted components of the C1s and O1s regions is given in Table 1.

Table 1 Summary of the fitted components of the C1s and O1s regions representing different carbon and oxygen species. The color code is used throughout the remainder of the study to easily separate the different species in the various figures

Binding energy (eV)	Spectral feature	Asymmetry parameter	FWHM (eV)	Color code	Ref.
	Full O1s intensity				
530.3	Cu_2O		~0.9		54 and 55
529.7	Cu_xO_y		~0.9		58
529.2	O_{ad}-like		~0.9		71
>530.4	C–O bonds				56 and 57
284.4	Free standing graphene/FLG	0.09/0.12	0.5–0.6		9
284.75	Coupled graphene	0.09	~0.6		9
284.0	Defects	0.09	~0.6		9
285.2	Rim of graphene domains	0.09	~0.6		9
284.8	sp^3 carbon				
>285.2	All C–O related bonds				

Note: C–O refers to all carbon oxygen related bonds, *e.g.* C–OH, C–O *etc.*

For semi-quantitative analysis, the relative abundance (in %) of carbon and oxygen for the various samples was calculated from the measured O1s and C1s intensities weighted by their respective escape depth and photoionization cross section. The Cu abundance was neglected because of the lack of information on absolute carbon coverage which would potentially lead to an overestimation of the Cu contributions. Contributions of specific components were calculated by considering the respective fractions obtained from the best fits with respect to the total intensity of each spectrum. The error is estimated to be ≈20% of the relative abundance.

Changes of the sample's WF were determined in a similar mode to the XPS experiments. The sample's Fermi edge at E_F as well as the secondary peak of inelastically scattered photoelectrons were recorded at a photon energy of 100 eV for two different analyzer pass energies and the WF calculated by $\varphi = h\nu - E_{max}$ with E_{max} being the point of inflexion of the secondary peak. Based on the obtained data sets of both analyzer pass energies the WF's uncertainty was estimated to be ≈0.05 eV.

The soft X-ray absorption spectra of the oxygen K-edge were recorded in the Total Electron Yield (TEY) in vacuum *via* the drain current of the sample induced by the incident photons. To ensure reproducibility, three scans were recorded separately for each spectral region. Background correction and normalization were carried out with respect to a spectrum of an oxygen free sample obtained at T = 600 °C.

The SEM micrograph of Fig. 1a was taken with a Zeiss Sigma VP at an accelerating voltage of 2.0 kV in-lens mode at a working distance of 6.8 mm. SEM micrographs of Fig. 1b and 7a–c and ESI,† Fig. S2 were recorded with a Hitachi S-4800 (FEG) at an accelerating voltage of 2.5 kV and 3 kV (ESI,† Fig. S2b) in SE mode using the upper and lower detector as one at a working distance of 8 mm. EDX spectra were recorded with an EDAX Sapphire Si(Li) detector and the EDAX software Genesis Version 6.39 at accelerating voltages of 3 kV (Fig. 1c and ESI,† Fig. S2b) and 5 kV (ESI,† Fig. S2d). ESEM micrographs (Fig. 3) were obtained in a modified commercial ESEM (FEI Quantum 200, base pressure ≈1 × 10^{-5} Pa) with a heating stage, gas supply unit and a mass flow controller bank (Bronkhorst) allowing variable gas mixtures. All tubing inside and outside the ESEM is stainless steel. The vacuum system of the ESEM was modified for oil free pumping. Thermocouples were directly spot welded onto the Cu foil for temperature control. Samples were imaged in SE mode at an acceleration voltage of 5.0 kV using a standard Everhart–Thornley detector.

Results

Oxygen intercalation on MLG/Cu *vs.* GF/Cu

As grown graphene can be heavily influenced by exposure to ambient pressure conditions even at room temperature.[9]

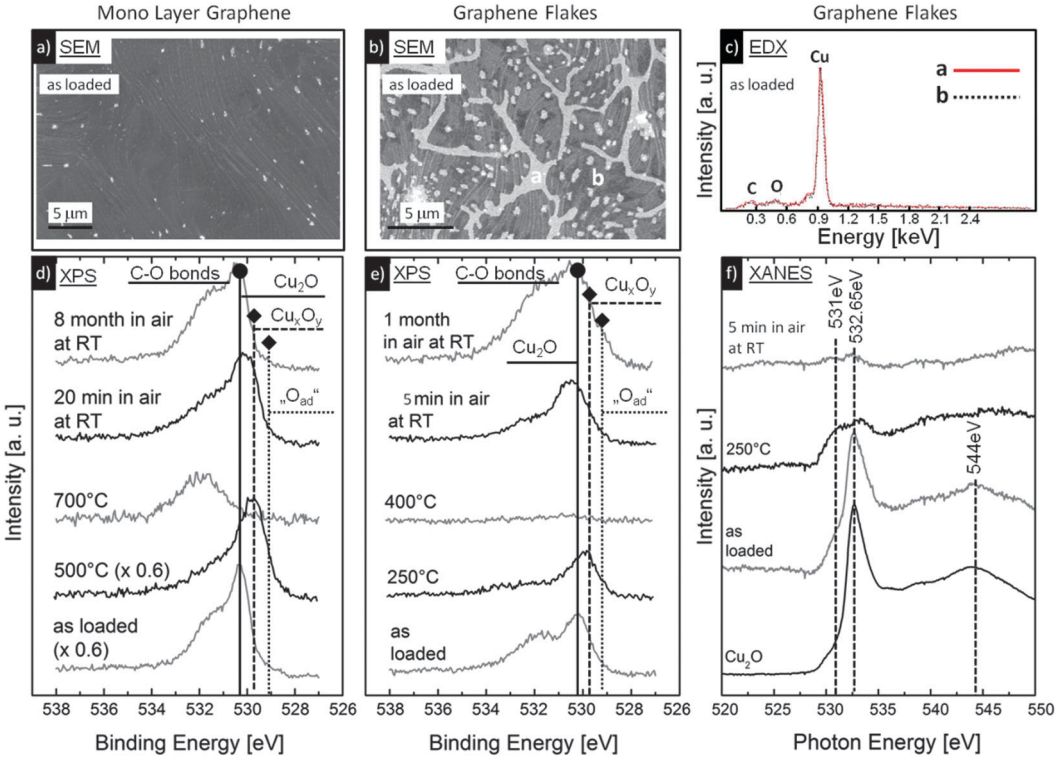

Fig. 1 Top panel: (a) SEM of as loaded MLG and (b) as loaded graphene flakes; (c) local EDX of as loaded GF taken in spots a (red) and b (black, dashed) of panel (b). Bottom panel: O1s spectra of MLG (d) and GF (e) before and during thermal treatment and subsequent air exposure, respectively. All carbon–oxygen related bonds are denoted as C–O bonds. (f) Oxygen K-edge XANES spectra corresponding to panel (e). Note: according to the results depicted in (e) virtually no oxygen (<1%) is present at $T \geq 400$ °C. Hence, the XANES spectra recorded at 600 °C were used for normalization to the photon flux in (f).

Usually, such samples are characterized using *ex situ* methods, which do not allow changes occurring on short time scales to be monitored. Hence, the as-prepared sample state may have changed without being noticed. To investigate the influence of the presence of oxygen on the graphene/Cu interface, long-term air stored (1 month) MLG and GF samples were systematically heated in vacuum and re-exposed to oxygen at RT and examined by means of SEM, EDX, and, *in situ*, by XPS and XANES.

While the SEM micrograph of as loaded MLG displays a homogeneously distributed graphene layer, the GF micrograph depicts bright uncovered Cu areas surrounding the GFs (Fig. 1a and b). We also note that the as grown GF also has holes within the islands. These holes are a result of the particular synthesis conditions used, similar to those observed in previous reports.[50] We explicitly select these "holey" GF samples for our study in order to enhance the contrast between a continuous MLG layer and the only fractional graphene island coverage of the holey GF. Underneath both, the MLG and the GFs, step-like facets of the Cu substrate can be seen in Fig. 1a and b which can arise from rolling striations in the foil.[51] On the other hand reconstructions of the underlying Cu layers occurring during growth and subsequent cooling may also contribute to their formation as reported by Han *et al.*[52] Interestingly, rather depth sensitive EDX (information depth ~ 1 µm) of the as grown GF sample (Fig. 1c) performed on the bare Cu rims and the GFs does not show any notable difference of the oxygen contribution on either of them. In contrast, a sample repeatedly reduced and re-oxidized exhibits a pronounced difference between the Cu and graphene areas, respectively. There, bare Cu areas exhibit a significantly increased EDX oxygen signal compared to graphene covered regions (ESI,† Fig. S2a and b). This finding suggests a protective function of graphene against oxidation of the underlying Cu substrate compared to the uncovered Cu areas.[36–39]

Considering the rather low surface sensitivity of EDX more sensitive XPS and XANES were applied to follow the oxygen related changes on graphene covered Cu in greater detail. Since after reduction, both, the Cu2p and Cu LMM regions are quite insensitive towards changes caused by small oxygen amounts, O1s spectra were taken for MLG and GF at a kinetic energy of the photo electrons (E_{kin}) of 150 eV (Fig. 1d and e).[9,53] Already the non fitted O1s spectra reveal distinct changes in the Cu–oxygen region ($\leq$530.3 eV) and the BE region dominated by various C–O related bonds (>530.3 eV, see Table 1) during all stages of sample treatment as indicated by the labelled markers.[54–57] When reaching a temperature of 500 °C (MLG) and 250 °C (GF), respectively, the initial centre of gravity of the Cu oxide contributions shifts toward a lower BE in the O1s which suggests a reduction of the Cu_2O to a sub oxide and subsurface oxygen.[58] With further heating to 700 °C and 400 °C, respectively, only minor C–O related components remain (MLG) or the O1s intensity has decreased to virtually zero (GF). Note that SEM images and EDX of the as loaded GF sample indicate sparsely distributed small Si oxide clusters on the sample surface most likely stemming from the manufacturing

process of the Cu foil despite its nominal purity of 99.999% (ESI,† Fig. S1c and d). However, since the corresponding O1s intensity of the GFs is virtually zero, we conclude that silica does not noticeably contribute to the O1s signal. Thus, the residual O1s intensities at 700 °C observed on the MLG sample are attributed to various C–O related bonds such as C–O, C═O, C–OH *etc.*[56,57] With re-oxidation for several minutes in air a partial recovery of the Cu_2O and C–O related bonds is observed on both samples. Extended air exposure ($t_{reox} \geq 1$ month) not only restores the initial sample state of both samples but seems to increase the C–O bond related intensities. The further impact of repeated reduction and re-oxidation on C and Cu is discussed in detail below.

For the GF sample a set of oxygen K-edge XANES spectra was also recorded during each preparation step (Fig. 1f). With heating to 250 °C, the Cu_2O-dominated as loaded XANES spectrum changes towards a spectrum resembling an adsorbate-like or a subsurface oxygen/sub-oxide state.[59,60] After removing all the oxygen at $T \geq 400$ °C (see Fig. 1e) and subsequent short re-oxidation the XANES spectrum indicates only a small recovery of oxygen compared to the spectrum recorded at 250 °C.

The results displayed in Fig. 1 involve methods with different information depths, ranging from a maximum depth of ~1 μm (EDX) over ~5 nm (XANES) to ~ 0.7–2 nm (XPS). From the combined data it is apparent that the observed oxygen contributions are located very near to or on top of the surface. For the C–O bond related features, for which the O1s region is extremely sensitive,[56,57] this was verified by XPS depth profiling which revealed different ratios between carbon–oxygen and Cu–oxygen related intensities dependent on the photo electron escape depth (ESI,† Fig. S3). Hence, the carbon–oxygen related contributions can be assigned to oxygen functionalities located at defects, edges and rims of the graphene. On the other hand Cu areas covered by graphene should be less oxidized because of the latter's protective coverage as evidenced by the EDX results presented in Fig. 1c and ESI,† Fig. S2a, particularly for short-term exposures.[36–39] Whereas the oxidized Cu signal on the GF sample may be explained by bare Cu surfaces exposed to ambient air this is not the case for the fully covered Cu on the MLG sample because of the lack of bare Cu areas. Diffusion of oxygen between the graphene and the Cu surface starting from the graphene rims inwards or from defect sites has to be taken into account, a process which would be enhanced for the GF sample because of a shorter diffusion length required to access the entire area underneath the graphene. This assumption is corroborated by the observed differences in the reduction temperature between MLG and GF samples similar to observations of graphene–oxygen–Ir systems.[10,61] The higher reduction temperature on MLG/Cu indicates a higher barrier to be overcome for a notable diffusion–reduction process. Thus, the changes in XP and XANES spectra upon reduction by heating and upon re-oxidation can be related to sub-oxide or adsorbate-like states, confirming the presence of intercalated oxygen atoms in the very early stage of oxidation and the very late stage of reduction. In later stages of the air exposure additionally Cu oxides are formed underneath the graphene.

Graphene–catalyst interaction

We now focus on the effect of reduction and re-oxidation on the C1s region in XPS. Fig. 2 shows a comparison of the C1s spectra of MLG/Cu and GF/Cu recorded during the same treatment as in Fig. 1d and e. Both samples behave very similar during heating and re-oxidation. The as loaded surfaces are dominated by a C1s main component at the typical graphite BE (284.4 eV).[62,63] The fitting parameters and asymmetric peak shape with $\alpha = 0.09$ are representative of ordered graphene.[64] We will address XP peak asymmetry in detail in the discussion. Several other minor intensity peaks are also present which can be assigned to contaminants related to air exposure such as C–O, C–OH bonds *etc.* (BE > 285.0 eV), sp^3 carbon (~284.8 eV) and defects in the graphene structure (284.0 eV).[56,65–68] In the best fit the peak shapes of the contaminants and sp^3 carbon lack the asymmetry found for graphene and graphitic carbon. Hence, they can be clearly distinguished from the asymmetric, shifted graphene

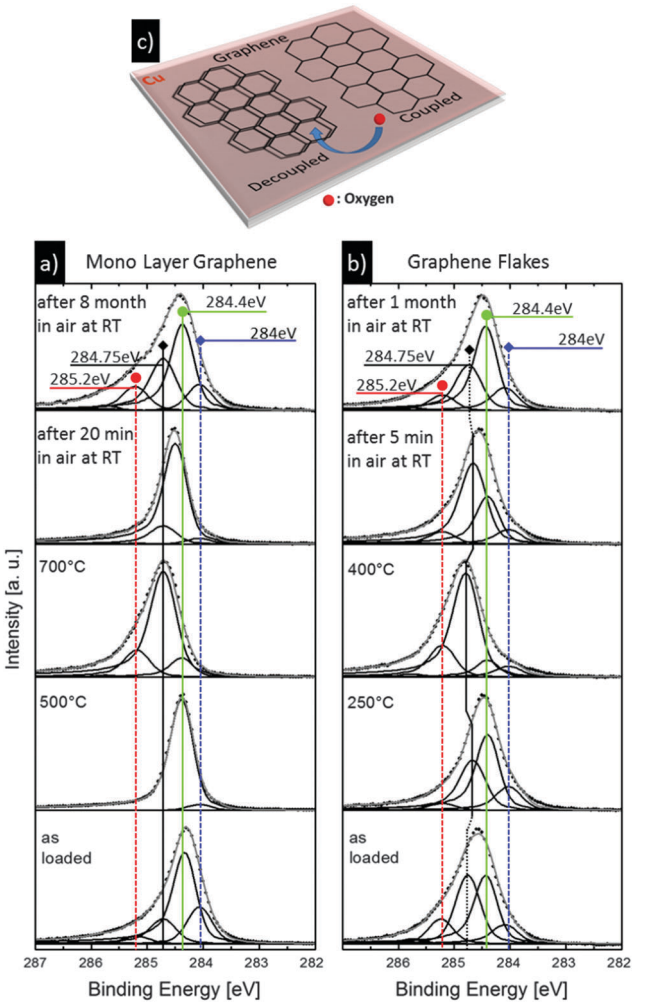

Fig. 2 Comparison of C1s spectra of aged MLG (a) and aged GFs (b), sample GFb (first cycle) before and during thermal treatment and subsequent air exposure, respectively. The temperature steps presented here mark the most drastic changes in the composition of the fitted components. (c) Schematic sketch of decoupling graphene.

peaks observed at the same BEs at higher sample temperatures when graphene is in direct contact with Cu (see below). In our experiments, the surfaces are cleaned by heating in vacuum above 250 °C to remove carbon adsorbates, various carbon–oxygen bonds and Cu_2O which is accompanied by an enhancement of the intensity of the 284.4 eV peak and, in the case of MLG, the loss of virtually all other peaks (second to bottom panel). This change coincides with the detection of sub-oxide/adsorbate-like states attributed to oxygen intercalation in the corresponding O1s spectra in Fig. 1. Further heating in vacuum leads to a distinctive shift of the main peak to a higher binding energy of 284.75 eV retaining an asymmetry parameter of $\alpha = 0.09$ which is indicative of a changed interaction between graphene and Cu. Only minor contributions at 284.4 and 285.2 eV are additionally observed. The 284.75 eV component has also been observed during MLG growth, and hence is assigned to as grown graphene in direct contact with Cu (*i.e.* without oxygen present). In contrast, the 285.2 eV component was previously attributed to sp^3 carbon bonds in the graphene affected by the altered interaction with the substrate.[9] Note that the shift of C1s majority BEs occurs already at a lower temperature on the GF sample together with the complete loss of oxygen (see Fig. 1e). Subsequent cooling of the samples in vacuum and leaving it at RT does not affect the C1s spectra at all (not shown).[9] Re-oxidation of the MLG and GFs at RT in ambient air for 20 and 5 min, respectively, leads to an inverse BE shift of the main intensity towards 284.4 eV which confirms a direct correlation of oxygen intercalation between Cu and graphene with the observed BE shifts. However, for the short exposure times displayed here the shift is not complete. A full recovery of the as loaded peak position would require a higher oxygen dose as confirmed by the 284.4 eV dominated spectra taken after $t_{reox} \geq 1$ month.

Both the MLG and the GF exhibit the observed changes in the C1s and O1s regions, with the GF being more sensitive to oxygen related changes. As apparent from the results displayed in Fig. 1 and 2, reduction and re-oxidation related processes such as the C1s BE shifts and O1s intensity changes not only occur already at lower T for the GF but also show a dependence on the oxygen dose. This further confirms the different diffusion lengths for MLG compared to GF. Thus, removal of oxygen on MLG/Cu requires a longer time or more aggressive conditions.

The difference in diffusion length and temperature stability of the intercalation process is further studied by heating air exposed continuous MLG and GF samples in vacuum while monitoring surface changes with ESEM. This allows laterally resolved visualization of changes caused by the interaction between the graphene and catalyst surface. Fig. 3a depicts a set of ESEM micrographs of a previously air exposed MLG

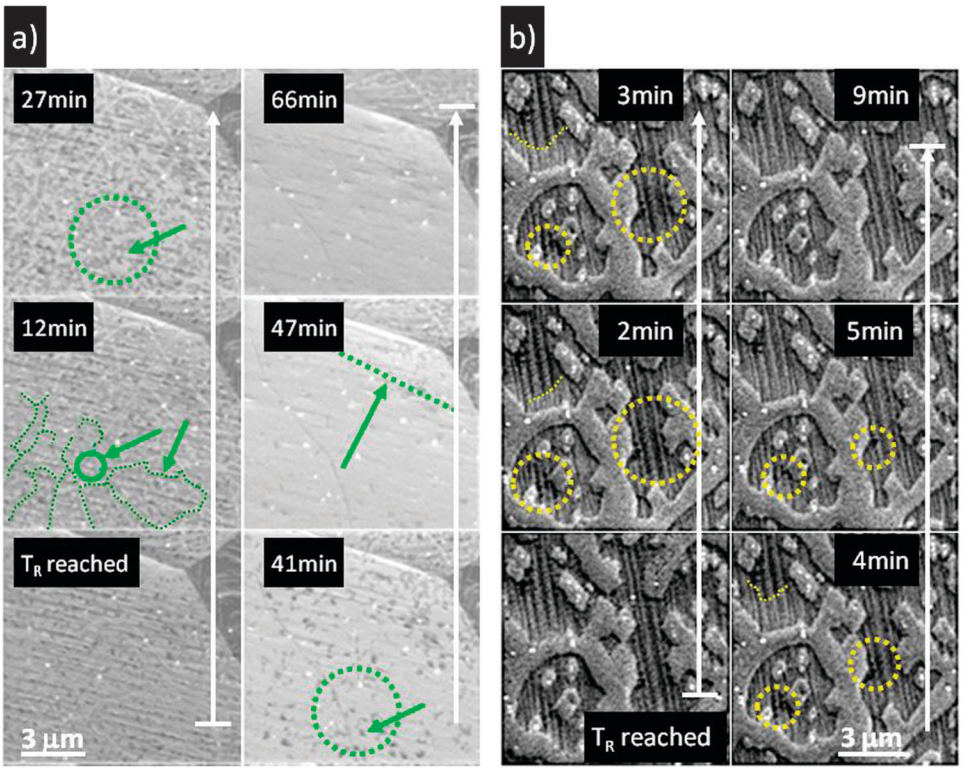

Fig. 3 (a) ESEM micrographs of MLG/Cu heated to and kept between ≈470 and 485 °C in vacuum for 66 min. Note that the whole heating process took ≈250 min starting from RT to completed contrast changes in the last image at ~480 °C. (b) ESEM micrographs of a GF/Cu heated to and kept between ≈380 to 395 °C in vacuum for 9 min with slowly increasing temperature. The image contrast was enhanced for better visibility of contrast changes. GFs appear as darker, striped areas surrounded by brighter ring- and finger-like Cu areas. Changes in contrast already occurred during heating which took ≈34 min from RT to 395 °C in the last image. Distinct contrast changes in (a) and (b) are marked (see text for details).

sample on polycrystalline Cu foil held at an average temperature of ≈480 °C in vacuum over a time of 66 minutes. Cu grain boundaries can be seen in the upper part of the images. Within the Cu grains faceting can be identified by the horizontal stripes in the very first image (Fig. 3a); lower left in agreement with the SEM results presented in Fig. 1a and b.[51,52] With ongoing heating small bright features appear in the rather homogeneous contrast within the Cu grains (12 min, Fig. 3a). Most of the bright structures enclose a relatively large area while others appear rather point-like. Hence, the former are attributed to graphene grain boundaries while the latter are most likely related to point defects in the graphene. Both features expand until they meet leaving only some small residual dark regions (27 min and 41 min). These changes are marked by circles and arrows in the figure. We attribute these changes to the beginning of de-intercalation of the oxygen atoms intercalated between graphene and Cu as observed above with XPS. This explanation is reasonable given the observed gradual changes point to the outward diffusion of oxygen atoms at graphene grain boundaries and defects.[6,69] Such a process would firstly cause a gradual depletion of the areas located close to grain boundaries and defect sites hence explaining the observed expansion of the bright features. This stage of de-intercalation proceeds slowly at roughly 2×10^{-3} μm s^{-1} at the given temperature. With prolonged heating, the ESEM micrographs change again in the form of a distinct contrast change moving over the Cu grains similar to a reaction front (dotted line at 47 min in Fig. 3a; ESEM movie in ESI†). Note, that the reaction front crosses readily over the Cu grain boundaries at a speed of approximately 40×10^{-3} μm s^{-1}. The time resolved ESEM movie reveals several details which exclude the possibility of this observation being related to an experimental artefact: firstly, the direction of the front changes when it crosses Cu grain boundaries which points to preferred directions of propagation. Secondly, within a Cu grain the front does not proceed uniformly but the propagation seems to be hindered by areas of darker contrast (*e.g.* dark area in the centre of the central Cu grain in ESEM movie). A possible explanation for this behaviour may be the removal of oxygen atoms with a longer residence time between graphene and Cu, *e.g.* those underneath the center of a graphene grain. The ultimate depletion of the last remaining oxygen may proceed along the main crystallographic orientations of the Cu substrate and cause the graphene to finally settle in registry with the Cu surface or the Cu surface may reconstruct in the absence of oxygen at the given temperature.[52,69–72] However, a detailed investigation of this phenomenon would require time and spatially better resolved structural methods such as AFM or STM which are beyond the scope of the present work.

The GF counterpart behaves similarly with respect to the changing contrasts (Fig. 3b). Again, with ongoing heating contrast changes are observed starting at flake edges and moving through the GFs. This is best seen in upper left GF marked by a dashed line. For the other GFs, the trench-like contrast of dark and bright stripes is attenuated and dark, defect-like spots vanish as marked by dashed circles. The de-intercalation proceeds rather uniformly without any reaction-front-like contrast change as observed after ~47 min for MLG on Cu. Compared to the heating time and temperature of the MLG on Cu (66 min, $T_R \approx 480$ °C) the time scale of less than 10 min at $T_R \approx 400$ °C required for the contrast changes of GF on Cu is notably shorter yielding in a de-intercalation speed of roughly 5–8 $\times 10^{-3}$ μm s^{-1} as derived from Fig. 3b. The comparison of GF and MLG on Cu in Fig. 3 implies that for MLG on Cu not only are the diffusion lengths different, depending mainly on the graphene coverage, but also the diffusion pathways. Considering the observed reaction front for MLG on Cu, the underlying Cu substrate's crystallographic orientation and its defect density may influence the oxygen de-intercalation as well. Thus, de-intercalation would require more time and/or a higher temperature for MLG than for GFs as observed in Fig. 3. These results are in excellent agreement with the XPS results depicted in Fig. 1 and 2 and confirm the suggested different diffusion lengths for MLG and GFs on Cu. The contrast changes from dark to bright presented in Fig. 3 are clearly related to the increased interaction between the Cu substrate and graphene observed with XPS above. The darker contrast in the presence of intercalated oxygen can be explained by a lower secondary electron yield due to the reduced contact between Cu and MLG which would be reflected as a change in WF.[73] In contrast to the strongly interacting or "coupled" graphene–Cu, when intercalated oxygen is present graphene on Cu can be considered as free standing in terms of its electronic properties.

To determine the activation energy required to intercalate/de-intercalate oxygen long term air stored GF/Cu samples were examined. Firstly, intercalated oxygen was removed by heating the samples in vacuum. Then, the process was reversed by stepwise heating the samples during oxygen exposure at three different pressures ($p_{O_2} = 5 \times 10^{-5}$, 5×10^{-2} and 0.2 mbar). During both treatments the changes in the C1s region were carefully monitored by XPS. The evolution of the different components is shown in Fig. 4 for an oxygen exposure of 0.2 mbar. As is obvious from the intensity changes with increasing temperature under the given conditions several partially overlapping processes have to be taken into account. Firstly, between 180 °C ≤ T ≤ 280 °C there is a sharp drop in intensity of the peak at 284.75 eV and a simultaneous increase in the peak intensity at 284.4 eV, which is representative of the intercalation of oxygen. Interestingly, in this set of experiments the temperature region for intercalation was found to be independent of the oxygen pressure suggesting a primarily kinetically driven intercalation process determined by the diffusion length of oxygen atoms. Note that the temperatures observed for de-intercalation in vacuum were within the range of 300 to 400 °C in agreement with the GF samples presented in Fig. 1 and 2. The second process sets in at temperatures above 280 °C for which a strong decrease of the overall C1s signal was observed which is related to etching of the graphene. In contrast to the intercalation, the onset of carbon etching turned out to be strongly dependent on the applied oxygen pressures: the lower the pressure the higher the required temperature with 5×10^{-2} mbar/≈450 °C and 5×10^{-5} mbar/≈500 °C found for

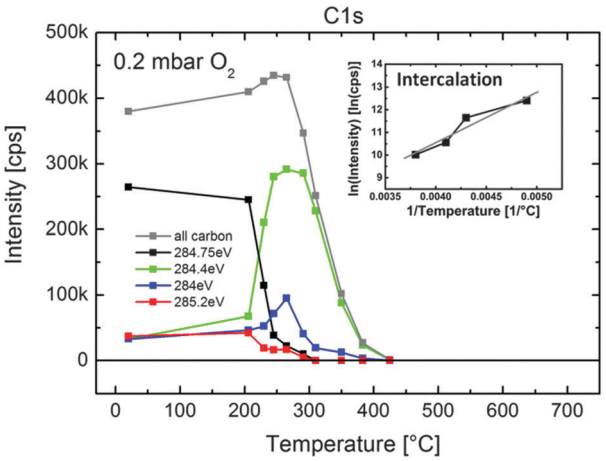

Fig. 4 Evolution of the relative abundance of the different carbon species of a GF/Cu sample during heating in 0.2 mbar oxygen as derived from fits of C1s spectra according to Table 1. Prior to the experiment shown here the intercalated oxygen of the initially long term air stored GF/Cu sample was removed by heating up to 600 °C in vacuum. The inset shows the Arrhenius plot of the graphene component at 284.75 eV derived from the narrow intercalation region between ≈200–280 °C.

the other two experiments, respectively (ESI,† Fig. S4b). Note that the peak shapes of the fitted components, in particular the 284.4 eV peak, do not change during etching (ESI,† Fig. S4a). Furthermore, small changes in the 284.0 and 285.2 eV peaks are observed which are most likely related to healing/removal of defect sites which can proceed by an increased mobility of single carbon atoms but also by burning. The latter effect will be addressed in more detail below.

While for the evaluation of the activation energy of etching graphene the overall C1s intensity can be used, a reasonable estimate of the activation energies of intercalation has to be independent of the observed simultaneous changes (see ESI,† Fig. S4 for further details). Hence, only the intensity change of the 284.75 eV component during heating in oxygen was taken into account because, as apart from its intensity decrease, it is virtually unaffected by any other oxygen induced change. Assuming a linear proportion of carbon and intercalating oxygen, analysis of the resulting Arrhenius plots (see inset in Fig. 4) yielded an activation energy for intercalation of $E_{\text{Act-intercal}}$ = 0.19 eV.[44] Similarly, the activation energy of de-intercalation of oxygen was determined during the initial heating of the same sample in vacuum yielding $E_{\text{Act-deintercal}}$ = −0.18 eV, which nicely reflects the reversibility of the process (see ESI,† Fig. S4c). The values are smaller than those found for oxygen intercalation on graphene–Ru systems pointing to a relatively weaker interaction between the graphene and the Cu substrate.[18] However, the activation energies are well within the range found for the intercalation of various compounds and atomic species in graphite.[74,75] Activation energies calculated for etching of graphene resulted in two different values of $E_{\text{act-etch}}$ = −1.14 eV and −0.44 eV for $p_{O_2} = 5 \times 10^{-5}$ and 0.2 mbar, respectively. While the former value is in good agreement with results from experiments performed on graphene–Ru systems under similar temperature and pressure conditions,[18,76] the latter has to be ascribed to the increased oxygen pressure. The higher pressure allows a more effective oxidation of the graphene which in turn leads to a faster carbon burn off in form of CO and CO_2 with increasing temperature.[77]

Finally, in contrast to the graphene layers and islands studied so far, in a complementary experiment we now examine long time air exposed few layer graphene (FLG) grown on polycrystalline Cu foil. The FLG was heated to 600 °C in vacuum and subsequently cooled to RT while depth profiling of the sample with *in situ* XPS at two different photon energies. Cu LMM and O1s spectra indicate only very small contributions of Cu oxide and carbon–oxygen related bonds for the as loaded sample compared to MLG and GFs (ESI,† Fig. S5 and Fig. 1d and e). This implies relatively stronger protection of the underlying metal from oxidation due to the multiple graphene layers.[38] Thereby, the carbon–oxygen related bonds reside on the carbon surface as inferred from a higher C–O– to Cu oxide ratio in the surface compared to the depth sensitive O1s spectra. Depth profiling of the C1s region is shown in Fig. 5a and b. As expected, the surface sensitive spectrum is dominated by the graphitic component at 284.4 eV accompanied by a considerably smaller peak at 284.75 eV and minor contributions at 284.0 and 285.2 eV. During heating and cooling the main intensities at 284.4 and 284.75 eV remain unaffected whereas the peak at 284.0 eV increases up to 600 °C and decrease again upon cooling. This behaviour can be attributed to a partial loss of carbon–oxygen bonds leaving defect sites on the carbon surface which slowly heal during the remaining heating/cooling treatment.[78–80] In contrast to the surface sensitive spectra, the spectra recorded at a higher photon energy are dominated by the 284.75 eV peak (Fig. 5b). Given the mean free path of ≈1.2 nm for the higher photon energy this increased signal reflects the binding energy of the carbon layer directly at the interface with Cu. With less access of oxygen to the Cu–carbon interface because of the protective adlayers above, the interaction strength between carbon

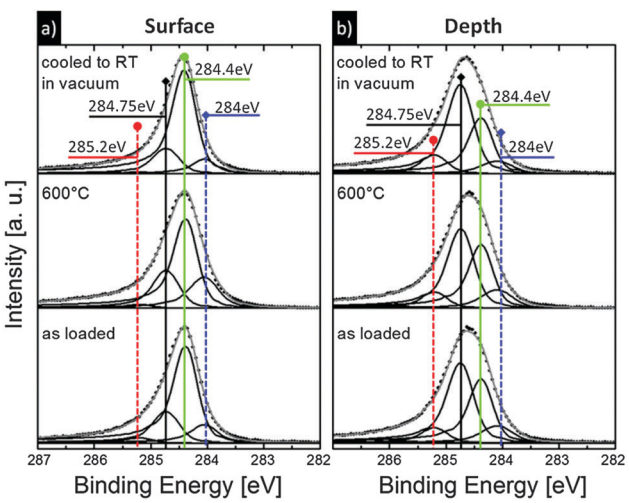

Fig. 5 Comparison of (a) surface (E_{kin} = 150 eV, corresponding to ~0.7 nm) and (b) depth sensitive (E_{kin} = 450 eV corresponding to ~1.5 nm) C1s spectra of FLG heated to 600 °C and subsequently cooled. The sample was kept in air for 1 month prior XPS analysis. The FLG consists of approx 3–4 layers.

and Cu remains the same as observed during growth under standard preparation conditions or after the removal of intercalated oxygen on MLG/Cu.[9] This indicates that for FLG only the electronic states of the layer directly located on the Cu is altered, while the upper layers retain electronic properties similar to free-standing graphene or graphite surfaces and remain unaffected by the Cu. Hence, the peak located at 284.75 eV represents the state of the first grown graphene directly on Cu, its "natural" state so to speak.[15] This is a further indication of the importance of oxygen intercalation in the creation of free standing graphene on Cu. Note that in the best fits presented in Fig. 5 the asymmetry of the fitted graphitic components is $\alpha = 0.09$ for the peak at 284.75 eV and $\alpha = 0.12$ for the peak at 284.4 eV, respectively (see Table 1). While the former value is identical to that typical of graphene the latter is clearly higher.[64] Yet, it is still below the asymmetry parameter commonly used for HOPG which is $\alpha = 0.15$. Since the asymmetry factor can be used as a rough measure to distinguish between graphene and graphite this difference indicates the gradual transition from graphene to graphite.[64] We will address this in the discussion in detail.

Aging by T–R-cycling and oxygen depth profiling

As apparent from the activation energy results presented above the integrity of graphene can be strongly affected by the presence of oxygen. Hence, graphene's potential degradation was examined by repeatedly reducing air stored GF/Cu samples in vacuum and subsequently exposing them to air again (T–R-cycling). GFs were chosen because of the more facile oxygen intercalation.

After storage in air for ≈3 month, a GF sample from the same batch as the sample used in Fig. 1 and 2 was T–R-cycled and then immediately cycled again (see ESI,† Table S1). The sample was then kept in air for ≈2 h and T–R-cycled again. The cycle-induced changes of the GF/Cu surface were monitored *in situ* with XPS. Resulting C1s spectra were fitted with the components summarized in Table 1. The corresponding O1s spectra were recorded at two different photon energies to account for depth and surface related variations in the oxygen species since a different distribution/concentration of certain species would be reflected by changes in the relative intensities of these species. For the spectral de-convolution several components with defined BEs accounting for various C–O bonds and Cu in various oxidation states were considered (see Table 1).[54–56,58,71] The comparison of O1s spectra taken during depth profiling reveals a strong similarity of spectral shapes and relative abundances of their fitted components for both photon energies (see ESI,† Fig. S3). Only the respective ratio between C–O and Cu related intensities differ slightly. This finding confirms the results depicted in Fig. 1 and 2 that all oxygen-related species reside very near to or on the sample surface manifested by Cu_xO_y and intercalated oxygen (rather than forming thick oxide layers) and by carbon–oxygen bonds directly on top of the graphene, respectively. Fig. 6a and b give an overview of the relative abundances of oxygen and carbon, respectively as calculated from their respective overall intensities. Whereas all Cu–oxygen related peaks in the O1s are completely quenched at 600 °C there always remain small intensities of carbon–oxygen related bonds. Interestingly, a short

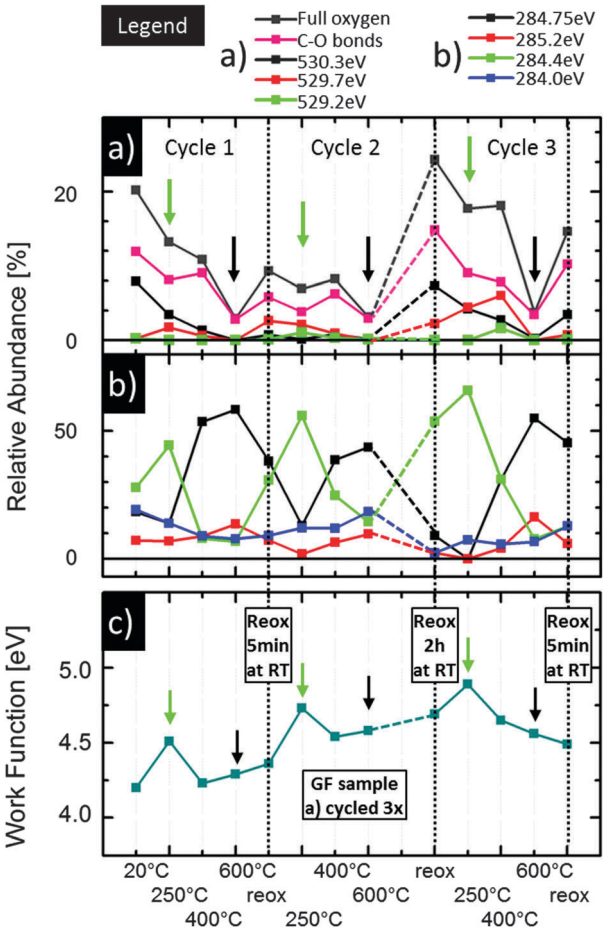

Fig. 6 Relative abundance derived from fits of sample GFa according to Table 1 of (a) different oxygen species during T–R cycling compared to the whole relative oxygen amount. Cu related components are given with separate BEs while all carbon–oxygen related (C–O) bond intensities are summarized. "Full oxygen" denotes the whole O1s intensity with respect to the total carbon intensity (in %). The Cu signal was neglected because of the lack of information on absolute carbon coverage. (b) Corresponding relative carbon abundances of the main C1s components. Note that carbon–oxygen bond related peaks are not included here. (c) Work function determined during each preparation step. Notes: (1) arrows indicate the most pronounced 284.4 eV (green) and 284.7 eV C1s peaks (black). (2) For reference the WF of polycrystalline Cu foil was determined as Cu_{Poly} = 4.65 eV.

re-oxidation time, *e.g.* at the beginning of cycle 2, leads only to sub-stoichiometric Cu oxide (529.7 eV) and adsorbate-like states (529.2 eV) while a longer air exposure such as that at the beginning of cycle 3 leads to a large fraction of Cu_2O.[54,55,58,71] Copper oxidation is known to proceed by atomic oxygen reconstruction of the copper surface and oxygen absorption into sub-surface regions, followed by nucleation of bulk Cu_2O phases.[81] The nucleation of Cu_2O is believed to occur after the saturation of sub-surface sites.[82] Once Cu_2O seeds have nucleated they grow laterally until the surface of the metal is covered by Cu_2O.[83,84] As seen in Fig. 1a a MLG sample with complete carbon coverage exhibits virtually the same evolution of O1s spectra as observed for GF on Cu only on a different temperature and time scale. This behaviour points to a comparatively fast onset of oxygen

adsorption/intercalation but to slow subsequent oxidation to Cu_2O because of the low temperature (RT) and limited oxygen supply by diffusion through different pathways, such as defects in the graphene layer.[85] This is corroborated by the results presented in Fig. 6a. Hence, in the present case a contribution of intercalating oxygen to the sub-oxide signal observed in the O1s spectra is obvious.

The corresponding C1s evolution appears even more versatile. After the first cycle, immediate re-oxidation leads only to a partial recovery of the peak at 284.4 eV which is completed by subsequent heating to 250 °C. Considering the changes of the O1s described above and the results presented in Fig. 4 this behaviour simply reflects the facilitated oxygen intercalation underneath the GF by thermal activation. A longer oxygen exposure time as performed between cycle 2 and 3 serves the same purpose. With an increasing number of cycles, the intercalation process seems to change as clearly indicated by the 284.4/284.7 peak ratio at each 400 °C step which increases with each cycle. Simultaneously, the intensities of the Cu–oxygen components at 400 °C (Fig. 6a) slowly increase as well. Both observations point to an easier access to and a longer retention time of oxygen at the GF/Cu interface.

As a well suited tool to monitor changes induced by adsorbate-like or suboxide states the integral (net-) WF was determined during each cycling step (Fig. 6c). Starting from 4.2 eV, the WF exhibits a gradual asymptotic increase throughout the three cycles. Superimposed on this "baseline" significantly higher values at each 250 °C heating step for all cycles are observed which decrease towards the baseline values already with the next heating step. Apparently, the WF maxima are a further fingerprint for the presence of intercalated oxygen which together with the first Cu layer can form a dipole increasing the barrier the escaping photo electrons have to overcome.

At $T > 250$ °C, the decrease in the WF reflects the stronger interaction between Cu and graphene due to removal of intercalated oxygen. These observations are also in good agreement with the ESEM results presented in Fig. 3. There, the changed WF manifested itself as a darker contrast related to a lowered secondary electron yield in the presence of intercalated oxygen.[73] Furthermore, since the reported WF for polycrystalline Cu is ≈4.65 eV, the comparatively low average values observed during the first cycle indicate a thin layered well ordered graphitic carbon, visible especially after removal of contaminants at 250 °C.[86] At this temperature, the WF is in good agreement with values reported in the literature for pristine graphene on Cu which is lower than that of multilayer systems such as multi walled carbon nanotubes or graphite.[87,88]

During cycle 2 and 3 with an increasing 284.4/284.7 peak ratio and larger amounts of residual Cu–oxygen at 400 °C the baseline of the WF increases as well to approx. 4.5 to 4.6 eV, the value of polycrystalline Cu. For a slightly differently treated sample (see ESI,† Table S1) the work function was determined even after a fourth and fifth cycle confirming the trends presented in Fig. 6c, namely a maximum at each 250 °C step coinciding with a distinguished C1s peak at 284.4 eV, followed by a decrease towards the baseline. The WF baseline values increase further reaching up to ∼4.8 eV (see ESI,† Fig. S6b). The latter value is in the range reported for oxygen adsorbed on polycrystalline Cu.[89] The reason for the increasing WF baseline seems to be more ready formation of Cu oxides (Cu_xO_y) during comparatively short air exposure (2 h) and their delayed removal during heating. Specifically, the oxygen content does not decrease as easily at $T \leq 400$ °C with increasing cycle number as visible in Fig. 6a for the third cycle. Both, the increasing WF and delayed reduction of Cu suggest an increase of bare Cu areas and thus, correspondingly, etching/burning off of carbon during repeated cycling.

Corroborating this, the carbon–oxygen bond related fractions of the O1s spectra are affected. With re-oxidation after cycle 2 an increase above the value of the as loaded sample is apparent which becomes pronounced again after the shorter re-oxidation at the end of cycle 3. This increase directly points to a GF degradation with increasing cycle numbers, presumably affecting mostly their outer edges and defect sites by etching through carbon oxidation/reduction. Corresponding Raman spectra indeed show an increase of the D peak indicating more defects in the graphene after three cycles (ESI,† Fig. S1). The GF degradation is nicely visible in Fig. 7. The comparison of the SEM micrographs of a non-cycled (Fig. 7a) and a 5 times cycled

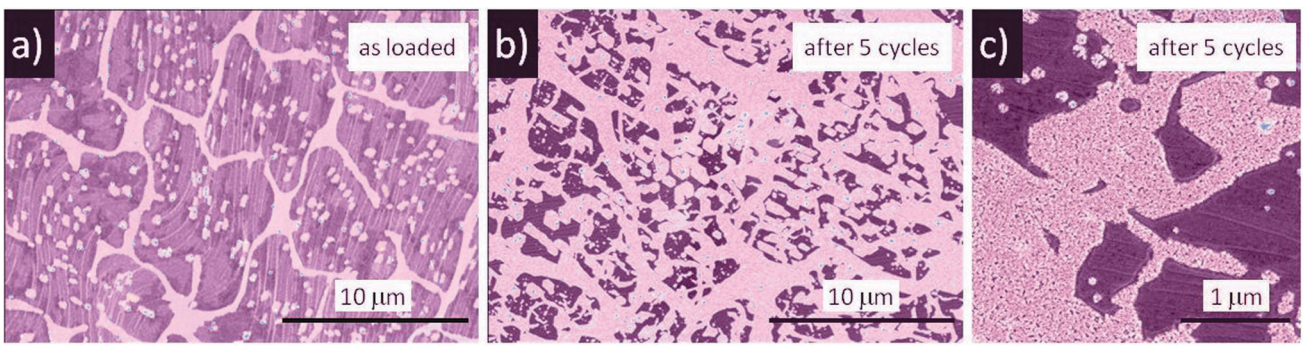

Fig. 7 SEM micrographs of (a) an as loaded GF/Cu sample kept in air for ∼3 month; (b) GF/Cu sample after 5 T–R cycles; (c) close up of oxidized Cu areas after 5 T–R cycles. The preparation conditions are described in detail in ESI,† Table S1. The images are colored for better contrast. Darker areas comprise of graphene, light pink marks bare Cu and Si oxide particles are white, partially inked in blue (see ESI,† Fig. S2).

sample (Fig. 7b, see ESI,† Table S1) not only reveals diminishing graphene flake areas (from ≈60 to ≈25% in the displayed area, also visible in corresponding Raman spectra by an increased Cu-to-carbon signal (ESI,† Fig. S1) but also degradation from within the flakes. The latter effect starts at the already present defect-like hexagonal holes of the non-cycled GFs.[50,90] These holes have grown considerably after five cycles, even partly retaining their shape. Note that the bare Cu areas of the cycled sample exhibit a more pronounced grainy structure pointing to a higher degree of Cu oxidation as shown in Fig. 7c and corroborating the SEM/EDX in ESI,† Fig. 2a and b.[91] Overall, the SEM confirms that a substantial fraction of the GF area was etched during the repeated T–R cycling, in excellent agreement with the XPS-inferred arguments above.

In correlation with the results presented in Fig. 4 etching/burning may prove an obstacle to the long term stability of graphene. On one hand etching by intercalated oxygen must be taken into account as recently suggested for graphene on Ir and Ru.[10,18,61,76] Defect sites on graphene may not only serve as access sites for intercalating oxygen but unsaturated carbon bonds in their vicinity may also be easily functionalized by the oxygen. Furthermore, the temperatures determined for thermal etching/burning of graphene are well within the range applied for de-intercalation. We want to emphasize that, as the annealing procedure is undertaken in vacuum of $\sim 10^{-8}$ mbar, the oxygen provided to etch the graphene is only supplied from below or adsorbed on the graphene, and not from the gas phase. As a consequence, with each cycle a partial loss of carbon by desorption of CO or CO_2 occurs. On the other hand, long-term exposure to ambient air leads to the formation of Cu_2O even in the presence of full MLG coverage. Recently, it was shown that such an oxidation of Cu can proceed *via* cracks between graphene islands and even be promoted by graphene *via* electrochemical reactions.[39,53] The oxidized Cu can serve as a reservoir for carbon oxidation when applying temperatures above RT which, in turn, cannot be so easily depleted as the graphene coverage becomes smaller after several T–R cycles. This also implies that the stability of air exposed MLG on Cu samples will depend on the reservoir size of oxygen (intercalated or from Cu–oxide) below the graphene and thus sample stability will be a function of exposure time to ambient air. From a technical point of view this finding is of great importance because it may strongly influence electronic applications or even transfer of graphene onto other substrates. In particular, temperature changes with and without atmosphere may cause unwanted damage.

Discussion

Graphene transfer and aging

The results presented above clearly show that interaction of oxygen with the graphene–Cu is quite complex and is dependent on the applied environmental conditions. While as grown graphene is rather strongly interacting with the Cu substrate, indicated by a higher C1s BE, air exposed graphene on Cu is not. However, the "as grown" graphene C1s BE can be re-established by removal of oxygen *via* vacuum annealing. This can, in turn, be again reversed by re-oxidation. This reversibility can be repeated several times, yet not without damage to the graphene. Consequently, a potential practical application of the oxygen intercalation to *e.g.* facilitate transfers of freshly grown graphene to other substrates requires a careful consideration of the pressure and temperature parameters to prevent damage of the graphene. The results presented in Fig. 4 and ESI,† Fig. S4 depicting the differences between (de-) intercalation and etching temperature at different oxygen pressures may serve as a guideline to find such conditions.

Graphene–Cu interaction

Similar effects of different graphene–substrate interactions in the presence of oxygen were observed for graphene on Ru and Ir and, most recently, Cu by Marsden *et al.* by combining ARPES and LEED.[9–11,14] In the latter work an ideal band structure around the *K*-point typical for free standing graphene was found when heating their sample to 200 °C. Regarding the results presented above (Fig. 2), this delay in observing a clear band structure can be explained by removing surface contaminations by thermal treatment. Further heating leads to an upward shift of the graphene's Dirac cone with respect to the Fermi energy E_F by ~ 0.35 eV. These results are in excellent agreement with our BE shift observed in the C1s spectra before and after oxygen removal at elevated temperatures schematically displayed in Fig. 8.

Generally, the rather large shift would imply a strong covalent-like bond between Cu and graphene which is obviously not the case as evidenced by the facile oxygen intercalation. A possible explanation for the observed behaviour is provided by the rigid band model in which the interaction between Cu and graphene is described by charge transfers causing an ionic bond without affecting the band structure. This model has been successfully applied to graphite–alkali systems, specifically HOPG/K.[92] In this system a charge transfer from K to graphite occurs which is accompanied by a distinct shift to higher BEs of ≈0.4 eV of the corresponding C1s peak with respect to clean HOPG. Furthermore, adsorbing oxygen on HOPG/K causes a backshift to the BE position of clean HOPG.[93] Viewing the Cu with its partly filled 4s state as a pseudo alkali metal a very similar situation would appear. The bond formed between Cu and graphene in the de-intercalated state would be similar to a Cu salt and could be easily dissociated by intercalating oxygen due to the stronger affinity of Cu to oxygen. However, to confirm this model detailed density of states calculations would be required which is beyond the scope of our present work. Hence, as a first approximation, the shift is interpreted as related to an n-type doping in the sense that the Cu substrate donates electrons to the graphene causing a shift of the Fermi edge relative to the Dirac point because of a change of the WF.[17,21,94] On the basis of DFT calculations Giovannetti *et al.* suggest a model which predicts the electron charge transfer for weakly adsorbed graphene, as is the case on Cu and several other catalysts, forming a dipole between graphene and substrate.[13] Our results show that with oxygen intercalation the charge

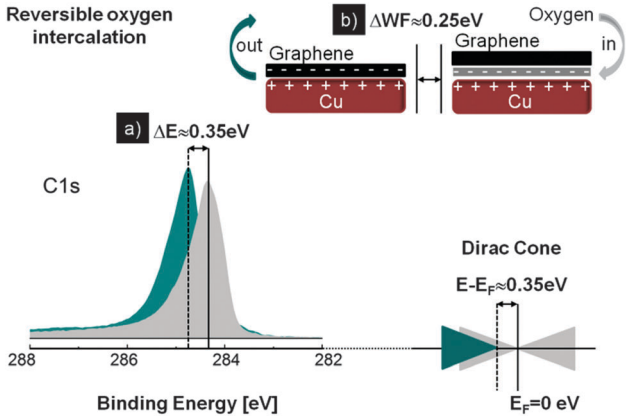

Fig. 8 Schematic overview of (a) the C1s BE shift between coupled and free standing graphene due to the presence of a charge transfer from Cu to graphene also visible in the changed position of the Dirac cone with respect to the Fermi edge (see ref. 14 for details) and (b) the influence of the presence of intercalated oxygen atoms on the dipole formation and hence WF changes of graphene–Cu.

transfer is interrupted when forming a graphene–O–Cu layered system in which graphene appears as quasi free standing, as evidenced by the BE shifted to the value common of graphitic carbon in various forms. The presence of intercalated oxygen prevents a charge transfer from the Cu substrate to the graphene. Instead the intercalating oxygen atoms replace the graphene as dipole partners with Cu which increases the WF compared to the oxygen free graphene–Cu system. However, the predicted WF change of graphene–Cu with respect to freestanding graphene of Giovannetti *et al.* is smaller compared to the results presented in Fig. 6c and ESI,† Fig. S6b. A simulation of Wang *et al.* on graphene–Ru provides a more detailed model including commensurability and local charge distributions between carbon and substrate atoms.[95] As a result it becomes clear that the experimentally obtained WF is a net value dependent not only on an increasing distance from the surface but on the integral charge distribution over different adsorption sites. Considering that the graphene on polycrystalline Cu does not necessarily grow epitaxially, which could already influence the BEs in the C1s region as observed for Ru, Rh and also Ni,[16,96] this may account for the observed larger ΔWF ≈ 0.25 eV between graphene in a coupled and in a free standing state created by intercalated oxygen.

Peak asymmetry of graphene

In contrast to the strong influence of intercalated oxygen on the WF and the BE shifts, the peak shapes used for fitting the C1s spectra remain mostly unaffected. Even after several T–R cycles accompanied by graphene degradation, the peak shape, largely dominated by its asymmetry, is retained. The asymmetry parameter α is an excellent fingerprint to divide sp^3 from sp^2, *i.e.* graphitic carbon, in graphene. While sp^3 carbon lacks any asymmetry, graphite exhibits a very well pronounced asymmetric tale, *e.g.* for HOPG a factor of $\alpha \approx 0.15$ is used.[63,97,98] Despite its long history, the origin of this asymmetry is still under discussion, *e.g.* by assigning it to localized sp^2-like defects in the sp^2 lattice induced by sputtering or rather disordered sp^3 carbon.[65,99] Also a functionalization by oxygen may increase the asymmetric line shape.[97] The most established opinion is that of final state effects due to relaxation and screening of the core hole left by the photo electron by intra- and interlayer processes similar to those in metals.[63,97,100] In a well ordered graphitic carbon system the 2p orbitals can overlap and delocalize.[62] The presence of defects and bonding to contaminants can disturb the delocalization leading to excitonic states which in turn have to be screened by other electrons to minimize the charging. This, in turn, leads to the observed asymmetry.[97,98] In the results presented above the main MLG and GF peak of air exposed, contaminant-free sample is located at 284.4 eV the established BE of graphitic carbon in a vast number of publications, *e.g.* ref. 62 and 63. The applied fitting procedure features an asymmetry parameter of $\alpha = 0.09$ confirming the presence of sp^2 carbon. This value is in very good agreement with results of Peltekis *et al.* who found with a combination of Raman, AFM and XPS, that such a low asymmetry factor is characteristic for well-ordered graphene grown on Cu during CVD.[64] Consistently, after removal of intercalated oxygen the best fit of the C1s peak at 284.75 eV is clearly asymmetric with $\alpha = 0.09$, hence still representing graphene strongly interacting with the Cu substrate. Interestingly, during further intercalation/de-intercalation cycles and even accompanying graphene degradation the peak shapes do not change. This finding is in opposition to the hypothesis of an increase of α because of screened defects and suggests that even under rather severe environmental conditions graphene may partially retain its electronic structure which may prove important for applications of *e.g.* nano-crystalline graphene in electronic devices.

Note that in the present work gradual changes of peak asymmetry were only observed with an increasing number of graphene layers (see Fig. 5). Again different explanations have been proposed for this behaviour, *e.g.* overlap of several carbon mono layer peaks or presence of a surface related spectral component due to relaxed binding conditions of the topmost carbon layer.[101,102] In the picture of the most established model presented above, a stronger influence of steps in a multilayered carbon system accounts for the asymmetry change.[57] Regarding the complex asymmetry changes displayed in Fig. 5 including strongly interacting graphene-like peak shapes for a component representing an interface layer with the substrate, this certainly requires a more detailed theoretical analysis. However, as a fingerprint to analyze samples for the presence and quality of graphene the value of asymmetry parameter can be used independent of its true physical origin.

Conclusions

In summary, it was shown that oxygen can intercalate between CVD grown graphene and the Cu substrate. This process is kinetically driven and depends mainly on the graphene coverage which determines the required time scale or temperature. For GFs, the activation energy was determined $E_{\text{Act-deintercal}} = -0.18$ eV $\approx E_{\text{Act-intercal}} = 0.19$ eV which is slightly lower than for

graphene–Ru. Oxygen intercalation leads to the formation of an adsorbate-like and/or Cu sub-oxide state which clearly inhibits the charge transfer between graphene and Cu directly observed after growth. In consequence, the as grown graphene electronically decouples from the Cu substrate towards quasi-free standing graphene which is not only reflected in a BE shift of the graphene C1s peak of $\approx$0.35 eV but also a distinct WF change by $\approx$0.25 eV. The oxygen intercalation is reversible and can be repeated several times even after long air exposures at RT.

In contrast, graphene etching was found to be strongly dependent on the applied oxygen pressure manifested by a lower activation energy for higher pressure. During repeated intercalation-de-intercalation cycles graphene etching notably increases, as confirmed by a considerable loss of graphene and an enhanced Cu oxidation because of the reduced protective graphene coverage. Whereas the structural integrity of the graphene with respect to coverage, flake size and defect growth is strongly affected by etching, based on XPS its key electronic properties are much less affected. The observed complex interplay of oxygen intercalation and electronic coupling effects of CVD graphene on Cu shows that there may be implications for processing graphene on the catalyst in integrated circuitry, when *e.g.* dedicated band structure alignment or metal contact passivation is required or for easier transfer to other substrates.[28–35] They also demand consideration when experimenting with nominally generic properties of graphene that is however air exposed on supports, such as graphene's debated wetting transparency and when considering graphene's debated use as a corrosion barrier.[36–43]

Acknowledgements

We thank the staff at BESSY II of the HZB for support and providing synchrotron light to our ISISS beamline. P.R.K. acknowledges the Lindemann Trust Fellowship. R.S.W. acknowledges a Research Fellowship from St. John's College, Cambridge. S.H. acknowledges funding from ERC grant InsituNANO (No. 279342) and EPSRC under grant GRAPHTED (Ref. EP/K016636/1). R.B. and A.K.-G. acknowledge funding from EU project GRAFOL, grant 285275.

Notes and references

1 H. Kim, C. Mattevi, M. Reyes Calvo, J. Oberg, L. Artiglia, S. Agnoli, C. Hirjibehedin, M. Chhowalla and E. Saiz, *ACS Nano*, 2012, **6**, 3614.
2 N. Wilson, A. Marsden, M. Saghir, C. Bromley, R. Schaub, G. Costantini, T. White, C. Partridge, A. Barinov, P. Dudin, A. Sanchez, J. Mudd, M. Walker and G. Bell, *Nano Res.*, 2013, **6**, 99.
3 T.-H. Han, Y. Lee, M.-R. Choi, S.-H. Woo, S.-H. Bae, B. Hong, J.-H. Ahn and T.-W. Lee, *Nat. Photonics*, 2012, **6**, 105.
4 S. Nie, J. Wofford, N. Bartelt, O. Dubon and K. McCarty, *Phys. Rev. B: Condens. Matter Mater. Phys.*, 2011, **84**, 155425.
5 J. Zhang, P. Hu, X. Wang and Z. Wang, *Chem. Phys. Lett.*, 2012, **536**, 123.
6 P. R. Kidambi, C. Ducati, B. Dlubak, D. Gardiner, R. S. Weatherup, M.-B. Martin, P. Seneor, H. Coles and S. Hofmann, *J. Phys. Chem. C*, 2012, **116**, 22492.
7 R. S. Weatherup, B. C. Bayer, R. Blume, C. Baehtz, P. R. Kidambi, M. Fouquet, C. T. Wirth, R. Schlögl and S. Hofmann, *ChemPhysChem*, 2012, **13**, 2544.
8 R. S. Weatherup, B. C. Bayer, R. Blume, C. Ducati, C. Baehtz, R. Schlögl and S. Hofmann, *Nano Lett.*, 2011, **11**, 4154.
9 P. R. Kidambi, B. C. Bayer, R. Blume, Z.-J. Wang, C. Baehtz, R. S. Weatherup, M.-G. Willinger, R. Schlögl and S. Hofmann, *Nano Lett.*, 2013, **13**, 4769.
10 R. Larciprete, S. Ulstrup, P. Lacovig, M. Dalmiglio, M. Bianchi, F. Mazzola, L. Hornekær, F. Orlando, A. Baraldi, P. Hofmann and S. Lizzit, *ACS Nano*, 2012, **6**, 9551.
11 P. Sutter, P. Albrecht, X. Tong and E. Sutter, *J. Phys. Chem. C*, 2013, **117**, 6320.
12 E. Granäs, M. Andersen, M. Arman, T. Gerber, B. Hammer, J. Schnadt, J. Andersen, T. Michely and J. Knudsen, *J. Phys. Chem. C*, 2013, **117**, 16438.
13 G. Giovannetti, P. Khomyakov, G. Brocks, V. Karpan, J. van den Brink and P. Kelly, *Phys. Rev. Lett.*, 2008, **101**, 026803.
14 A. Marsden, M.-C. Asensio, J. Avila, P. Dudin, A. Barinov, P. Moras, P. Sheverdyaeva, T. White, I. Maskery, G. Costantini, N. Wilson and G. Bell, *Phys. Status Solidi RRL*, 2013, **7**, 643.
15 X. Feng and M. Salmeron, *Appl. Phys. Lett.*, 2013, **102**, 053116.
16 M. Batzill, *Surf. Sci. Rep.*, 2012, **67**, 83.
17 A. Dahal, R. Addou, H. Coy-Diaz, J. Lallo and M. Batzill, *APL Mater.*, 2013, **1**, 042107.
18 P. Sutter, J. Sadowski and E. Sutter, *J. Am. Chem. Soc.*, 2010, **132**, 8175.
19 S. Lizzit, R. Larciprete, P. Lacovig, K. Kostov and D. Menzel, *ACS Nano*, 2013, **7**, 4359.
20 I. Jeon, H. Yang, S.-H. Lee, J. Heo, D. Seo, J. Shin, U.-I. Chung, Z. Kim, H.-J. Chung and S. Seo, *ACS Nano*, 2011, **5**, 1915.
21 A. Walter, S. Nie, A. Bostwick, K. Kim, L. Moreschini, Y. Chang, D. Innocenti, K. Horn, K. McCarty and E. Rotenberg, *Phys. Rev. B: Condens. Matter Mater. Phys.*, 2011, **84**, 195443.
22 L. Nilsson, M. Andersen, R. Balog, E. Lægsgaard, P. Hofmann, F. Besenbacher, B. Hammer, I. Stensgaard and L. Hornekær, *ACS Nano*, 2012, **6**, 10258.
23 S. Schumacher, T. Wehling, P. Lazic, S. Runte, D. Föster, C. Busse, M. Petrovic, M. Kralj, S. Blügel, N. Atodiresei, V. Caciuc and T. Michely, *Nano Lett.*, 2013, **13**, 5013.
24 N. A. Vinogradov, K. Schulte, M. Ng, A. Mikkelsen, E. Lundgren, N. Martensson and A. Preobrajenski, *J. Phys. Chem. C*, 2011, **115**, 9568.

25 D. Marchenko, A. Varykhalov, A. Rybkin, A. M. Shikin and O. Rader, *Appl. Phys. Lett.*, 2011, **98**, 122111.
26 R. Mu, Q. Fu, L. Jin, L. Yu, G. Fang, D. Tan and X. Bao, *Angew. Chem., Int. Ed.*, 2012, **51**, 4856.
27 D. Ma, Y. Zhang, M. Liu, Q. Ji, T. Gao, Y. Zhang and Z. Liu, *Nano Res.*, 2013, **6**, 671.
28 S. Song, J. Park, O. Sul and B. Cho, *Nano Lett.*, 2012, **12**, 3887.
29 F. Xia, T. Müller, Y.-M. Lin, A. Valdes-Garcia and P. Avouris, *Nat. Nanotechnol.*, 2009, **4**, 839.
30 C. Malec, B. Elkus and D. Davidović, *Solid State Commun.*, 2011, **151**, 1791.
31 H. Liu, H. Kondo and T. Ohno, *Phys. Rev. B: Condens. Matter Mater. Phys.*, 2012, **86**, 155434.
32 B. Dlubak, P. Kidambi, R. Weatherup, S. Hofmann and J. Robertson, *Appl. Phys. Lett.*, 2012, **100**, 173113.
33 B. Dlubak, M.-B. Martin, R. S. Weatherup, H. Yang, C. Deranlot, R. Blume, R. Schloegl, A. Fert, A. Anane, S. Hofmann, P. Seneor and J. Robertson, *ACS Nano*, 2012, **6**, 10930.
34 J. Meyer, P. R. Kidambi, B. C. Bayer, C. Weijtens, A. Kuhn, A. Centeno, A. Pesquera, A. Zurutuza, J. Robertson and S. Hofmann, *Sci. Rep.*, 2014, **4**, 5380.
35 A. Kuruvila, P. R. Kidambi, J. Kling, J. B. Wagner, J. Robertson, S. Hofmann and J. Meyer, *J. Mater. Chem. C*, 2014, **2**, 6940.
36 S. Chen, L. Brown, M. Levendorf, W. Cai, S.-Y. Ju, J. Edgeworth, X. Li, C. Magnuson, A. Velamakanni, R. Piner, J. Kang, J. Park and R. Ruoff, *ACS Nano*, 2011, **5**, 1321.
37 M. Schriver, W. Regan, W. Gannett, A. Zaniewski, M. Crommie and A. Zettl, *ACS Nano*, 2013, **7**, 5763.
38 D. Prasai, J. Tuberquia, R. Harl, K. Jennings and K. Bolotin, *ACS Nano*, 2012, **6**, 1102.
39 F. Zhou, Z. Li, G. Shenoy, L. Li and H. Liu, *ACS Nano*, 2013, **7**, 6939.
40 Z. Li, Y. Wang, A. Kozbial, G. Shenoy, F. Zhou, R. McGinley, P. Ireland, B. Morganstein, A. Kunkel, S. Surwade, L. Li and H. Liu, *Nat. Mater.*, 2013, **12**, 925.
41 R. Raj, S. Maroo and E. Wang, *Nano Lett.*, 2013, **13**, 1509.
42 J. Rafiee, X. Mi, H. Gullapalli, A. Thomas, F. Yavari, Y. Shi, P. Ajayan and N. Koratkar, *Nat. Mater.*, 2012, **11**, 217.
43 A.-Y. Lu, S.-Y. Wei, C.-Y. Wu, Y. Hernandez, T.-Y. Chen, T.-H. Liu, C.-W. Pao, F.-R. Chen, L.-J. Li and Z.-Y. Juang, *RSC Adv.*, 2012, **2**, 3008.
44 S. Tjandra and F. Zaera, *J. Vac. Sci. Technol., A*, 1992, **10**, 404.
45 A. Knop-Gericke, E. Kleimenov, M. Hävecker, R. Blume, D. Teschner, S. Zafeiratos, R. Schlögl, V. Bukhtiyarov, V. Kaichev, I. Prosvirin, A. Nizovskii, H. Bluhm, A. Barinov, P. Dudin and M. Kiskinova, *Adv. Catal.*, 2009, **52**, 213.
46 M. Seah, *Surf. Interface Anal.*, 1986, **9**, 85.
47 J. Yeh and I. Lindau, *At. Data Nucl. Data Tables*, 1985, **32**, 1.
48 D. Shirley, *Phys. Rev. B: Solid State*, 1972, **5**, 4709.
49 S. Doniach and M. Sùnjić, *J. Phys. C: Solid State Phys.*, 1970, **3**, 285.
50 Y. Zhang, Z. Li, P. Kim, L. Zhang and C. Zhou, *ACS Nano*, 2012, **6**, 126.
51 H. Wang, G. Wang, P. Bao, S. Yang, W. Zhu, X. Xie and W.-J. Zhang, *J. Am. Chem. Soc.*, 2012, **134**, 3627.
52 G. Han, F. Günes, J. Bae, E. Kim, S. Chae, H.-J. Shin, J.-Y. Choi, D. Pribat and Y. Lee, *Nano Lett.*, 2011, **11**, 4144.
53 I. Wlasny, P. Dabrowski, M. Rogala, P. Kowalczyk, I. Pasternak, W. Strupinski, J. Baranowski and Z. Klusek, *Appl. Phys. Lett.*, 2013, **102**, 111601.
54 J. Ghijsen, L. Tjeng, J. van Elp, H. Eskes, J. Westerink, G. Sawatzky and M. Czyzyk, *Phys. Rev. B: Condens. Matter Mater. Phys.*, 1988, **38**, 11322.
55 S. Poulston, P. M. Parlett, P. Stone and M. Bowker, *Surf. Interface Anal.*, 1996, **24**, 811.
56 J.-P. Tessonnier, D. Rosenthal, T. Hansen, C. Hess, M. Schuster, R. Blume, F. Girgsdies, N. Pfänder, O. Timpe, D. Su and R. Schlögl, *Carbon*, 2009, **47**, 1779.
57 B. Frank, A. Rinaldi, R. Blume, R. Schlögl and D. Su, *Chem. Mater.*, 2010, **22**, 4462.
58 H. Bluhm, M. Hävecker, A. Knop-Gericke, E. Kleimenov, R. Schlögl, D. Teschner, V. Bukhtiyarov, D. Ogletree and M. Salmeron, *J. Phys. Chem.*, 2004, **108**, 14340.
59 D. Vvedensky, J. Pendry, U. Döbler and K. Baberschke, *Phys. Rev. B: Condens. Matter Mater. Phys.*, 1987, **35**, 7756.
60 A. Knop-Gericke, M. Hävecker, T. Schedel-Niedrig and R. Schlögl, *Top. Catal.*, 2000, **10**, 187.
61 E. Granäs, J. Knudsen, U. A. Schröder, T. Gerber, C. Busse, M. Arman, K. Schulte, J. Andersen and T. Michely, *ACS Nano*, 2012, **6**, 9951.
62 H. Darmstadt and C. Roy, Letters to the Editor, *Carbon*, 2003, **41**, 2662.
63 P. van Attekum and G. Wertheim, *Phys. Rev. Lett.*, 1979, **43**, 1896.
64 N. Peltekis, S. McEvoy, K. Lee, A. Weidlich and G. Duesberg, *Carbon*, 2012, **50**, 395.
65 H. Estrade-Szwarckopf, *Carbon*, 2004, **42**, 1713.
66 N. McEvoy, N. Peltekis, S. Kumar, E. Rezvani, H. Nolan, G. Keeley, W. Blau and G. Duesberg, *Carbon*, 2012, **50**, 1216.
67 J. Lascovich, R. Giorgi and S. Scaglione, *Appl. Surf. Sci.*, 1991, **47**, 17.
68 A. Barinov, H. Üstünel, S. Fabris, L. Gregoratti, L. Aballe, P. Dudin, S. Baroni and M. Kiskinova, *Phys. Rev. Lett.*, 2007, **99**, 46803.
69 Y. Zhang, Q. Fu, Y. Cui, R. Mu, L. Jin and X. Bao, *Phys. Chem. Chem. Phys.*, 2013, **15**, 19042.
70 J. Tian, H. Cao, W. Wu, Q. Yu, N. Guisinger and Y. Chen, *Nano Lett.*, 2012, **12**, 3893.
71 K. Moritani, M. Okada, Y. Teraoka, A. Yoshigoe and T. Kasai, *J. Phys. Chem. C*, 2008, **112**, 8662.
72 L. Luo, Y. Kang, J. Yang and G. Zhou, *Surf. Sci.*, 2012, **606**, 1790.
73 J. Luo, P. Tian, C.-T. Pan, A. Robertson, J. Warner, E. Hill, G. Andrew and D. Briggs, *ACS Nano*, 2011, **5**, 1047.
74 H. Krohn, *Carbon*, 1985, **23**, 449.
75 J. Gonzalez Velasco, *J. Phys. Chem. Solids*, 1996, **57**, 857.

76 E. Starodub, N. Bartelt and K. McCarty, *J. Phys. Chem. C*, 2010, **114**, 5134.
77 T. Sun, S. Fabris and S. Baroni, *J. Phys. Chem. C*, 2011, **115**, 4730.
78 L. Tsetserisa and S. Pantelides, *Carbon*, 2009, **47**, 901.
79 C. Wang and Y.-H. Ding, *J. Mater. Chem. A*, 2013, **1**, 1885.
80 F. Ding, K. Jiao, Y. Lin and B. Yakobson, *Nano Lett.*, 2007, **7**, 681.
81 M. Lampimäki, K. Lahtonen, M. Hirsimäki and M. Valden, *J. Chem. Phys.*, 2007, **126**, 034703.
82 L. Li and G. Zhou, *Surf. Sci.*, 2013, **615**, 57.
83 J. Yang, B. Kolasa, J. Gibson and M. Yeadon, *Appl. Phys. Lett.*, 1998, **73**, 2841.
84 G. Zhou and J. Yang, *J. Mater. Res.*, 2005, **20**, 1684.
85 S. O'Hern, C. Stewart, M. Boutilier, J.-C. Idrobo, S. Bhaviripudi, S. Das, J. Kong, T. Laoui, M. Atieh and R. Karnik, *ACS Nano*, 2012, **6**, 10130.
86 M. v. Przychowski, G. Marx, G. Fecher and G. Schönhense, *Surf. Sci.*, 2004, **549**, 37.
87 A. Siokou, F. Ravani, S. Karakalos, O. Frank, M. Kalbac and C. Galiotis, *Appl. Surf. Sci.*, 2011, **257**, 9785.
88 H. Ago, T. Kugler, F. Cacialli, W. Salaneck, M. Shaffer, A. Windle and R. Friend, *J. Phys. Chem. B*, 1999, **103**, 8116.
89 G. Tibbetts, J. Burkstrand and C. Tracy, *Phys. Rev. B: Solid State*, 1977, **15**, 3652.
90 T. Maa, W. Rena, X. Zhang, Z. Liua, Y. Gaoa, L.-C. Yina, X.-L. Maa, F. Ding and H.-M. Cheng, *Proc. Natl. Acad. Sci. U. S. A.*, 2013, **110**, 20386.
91 Y. Zhou and J. Switzer, *Mater. Res. Innovations*, 1998, **2**, 22.
92 P. Bennich, C. Puglia, P. A. Brühwiler, A. Nilsson, A. Maxwell, A. Sandell, N. Martensson and P. Rudolf, *Phys. Rev. B: Condens. Matter Mater. Phys.*, 1999, **59**, 8292.
93 C. Puglia, P. Bennich, J. Hasselström, P. Brühwiler, A. Nilsson, Z. Li, P. Rudolf and N. Martensson, *Surf. Sci.*, 2001, **488**, 1.
94 M. Copuroglu, P. Aydogan, E. Polat, C. Kocabas and S. Süzer, *Nano Lett.*, 2014, **14**, 2837.
95 B. Wang, S. Günther, J. Wintterlin and M.-L. Bocquet, *New J. Phys.*, 2010, **12**, 043041.
96 L. L. Patera, C. Africh, R. S. Weatherup, R. Blume, S. Bhardwaj, C. Castellarin-Cudia, A. Knop-Gericke, R. Schlögl, G. Comelli, S. Hofmann and C. Cepek, *ACS Nano*, 2013, **7**, 7901.
97 T. Cheung, *J. Appl. Phys.*, 1982, **53**, 6857.
98 A. Chakraborty, R. Woolley, Y. Butenko, V. Dhanak, L. Siller and M. Hunt, *Carbon*, 2007, **45**, 2744.
99 D.-Q. Yang and E. Sacher, *Surf. Sci.*, 2002, **504**, 125.
100 G. Mahan, *Phys. Rev.*, 1967, **163**, 612.
101 D.-Q. Yang and E. Sacher, *Langmuir*, 2006, **22**, 860.
102 G. Speranza and L. Minati, *Surf. Sci.*, 2006, **600**, 4438.